

Journal of
Mechanics of
Materials and Structures

**RANDOM FIELD AND HOMOGENIZATION FOR
MASONRY WITH NONPERIODIC
MICROSTRUCTURE**

Vittorio Gusella and Federico Cluni

Volume 1, N° 2

February 2006

RANDOM FIELD AND HOMOGENIZATION FOR MASONRY WITH NONPERIODIC MICROSTRUCTURE

VITTORIO GUSELLA AND FEDERICO CLUNI

The purpose of this paper is to illustrate a method for homogenizing masonry with a nonperiodic microstructure. The proposed approach is based on the concept of the representative volume element and on the finite-size test-window method. First, the peculiarities of masonry as a composite continuum are highlighted. Then, the heterogeneity of the microstructure (elements and texture) is modeled by statistical descriptors. To improve the classical test-window method a probabilistic convergence criterion is coupled with the well-known mechanical convergence criterion. Both criteria must be met in order to check the convergence of the material window with the statistically equivalent representative volume element. An application shows the effectiveness of the proposed approach.

1. Introduction

Within the framework of micromechanics theory, masonry is modeled as a heterogeneous material composed of bricks or stones in a matrix of mortar. In dealing with a heterogeneous continuum, homogenization techniques allow one to define an equivalent body in order to study linear and nonlinear behavior [Christensen 1980; Suquet 1987].

The application of this approach to masonry was proposed by Pande et al. [1989], Pietruszczak and Niu [1992], and Maier et al. [1991]. On the basis of asymptotic analysis [Bensoussan et al. 1978; Sanchez-Palencia 1980], a rigorous application of the homogenization theory to periodic media was developed by Anthoine [1995]. The effect of rigid or elastic blocks was analyzed by Cecchi and Sab [2002], while failure analysis, ultimate strength, and damage models were considered in [Alpa and Monetto 1994; De Buhan and De Felice 1997; Luciano and Sacco 1997], respectively.

The hypothesis of a “periodic microstructure” in masonry has been adopted in all previous papers. This means that the bricks and the mortar joints are assumed to be of equal dimensions and characteristics. Moreover, these elements must be arranged in a periodic pattern.

Keywords: masonry, random heterogeneous material, homogenization.

However, the most interesting aspect of masonry structure analysis is related to the maintenance and restoration of historical and monumental buildings. In these cases the assumption of a periodic microstructure in stone masonry or brickwork would be mistaken. In order to apply the homogenization theory to old masonry it is necessary to use a different approach.

This aspect was considered in [Cluni and Gusella 2004], where the representative volume element of the masonry wall was determined by employing a formulation based on finite-size test-windows. In analyzing a masonry wall, the homogenized medium elastic stiffness tensor was obtained by considering the hierarchy of estimates relative to essential and natural boundary conditions. An adequate linear model for masonry is very important, because it permits one to analyze very large structures (monumental and historical buildings), and indicates those parts that bear the greatest stresses, where one must consider a more sophisticated nonlinear analysis.

A different procedure was proposed by Šejnoha et al. [2004] to analyze masonry structures with irregular geometry. This methodology, based on [Povirk 1995] and further developed in [Zeman and Šejnoha 2001; Šejnoha and Zeman 2002], introduces a periodic unit cell that possesses statistical proprieties similar to the original material and can therefore be considered a reasonable approximation.

In [Cluni and Gusella 2004], the material window is considered an adequate estimation of the representative volume element when the difference between natural and essential elastic moduli is limited. However, an estimation of the representative volume element based solely on mechanical convergence may be inaccurate. It is necessary to check that this convergence does not reflect the conditions in a specific portion of the wall in question and that the test-window is sufficiently representative of the masonry in terms of its constituent elements (stones and mortar joints) and its texture.

For particular composites, this aspect was highlighted by Bochenek and Pyrz [2004], who introduced statistical and geometrical measures and constraints to reconstruct families of plane and spatial dispersion of inclusions resembling reference patterns and to predict overall properties. Introducing the concept of peridization, the combination of mechanical and statistical criteria was also proposed in [Sab and B. 2005].

This paper proposes an improvement of the finite-size test-window method in order to overcome these limitations of the representative volume element estimation based solely on the mechanical convergence criterion. First, the peculiarities of masonry, which are related to the construction technique employed, are highlighted. Nonperiodic masonry is then analyzed within the framework of random heterogeneous material theory, and statistical descriptors are introduced in order to describe the random field modeling of masonry. Mechanical and probabilistic



Figure 1. Portion of the medieval defense walls of an Italian town. Note that the hypothesis of periodic continuum is not applicable.

criteria are used to check the convergence of the material window to the statistical equivalent volume element. These criteria are illustrated by applying them to an actual masonry wall.

2. Masonry as a peculiar heterogeneous material

Masonry can be considered a heterogeneous material composed of stones or bricks in a matrix of mortar. However it is a very particular composite: taken together, the inclusions (bricks or stones) have a much larger surface area than the matrix (in the case of dry masonry the matrix disappears); the mortar could in fact be regarded as merely joining the inclusions; the constituent blocks and mortar joints have different dimensions.

Leaving aside very chaotic typologies, some regularity is imposed by the building procedure even in stone masonry (see, for example, [Figure 1](#)):

- the masonry is built with courses of blocks connected by head and bed mortar joints;
- the bed mortar joints are continuous and more or less horizontal;
- the bed thickness is fairly constant for each course;

- the head joints are almost always interrupted vertically by inclusions;
- the inclusions are roughly rectangular;
- blocks belonging to the same course have similar dimensions, especially the heights, inasmuch as the bed joints are horizontal;
- there is no relation between consecutive courses, in fact their heights are purposely differentiated so as to obtain good quality masonry (in practice courses with larger stones are not grouped together but more or less evenly distributed vertically).

These features give the *masonry pattern* (or *masonry texture*) which characterize the mechanical behavior of the wall.

Given that the hypothesis of periodic continuum is not applicable, an important issue, in order to define a homogeneous continuum equivalent to the masonry, is the minimum size of the representative volume element [Drugan and Willis 1996].

Based on these observations, acceptance of a volume as being representative requires a set of conditions which are both mechanical and probabilistic. Thus the masonry wall must be analyzed within the framework of random field theory.

3. Masonry random field

Consider the masonry as a random heterogeneous material or simply a random medium [Torquato 2001]. A masonry wall is a realization of this two-phase random medium and occupies a region $\mathbf{D} \subseteq \mathbb{R}^2$ that is partitioned into two disjoint random sets or phases (we consider here the mechanical and probabilistic problems in 2-dimensional terms; however, the proposed approach can be extended to the third dimension).

Let \mathbf{D}_1 be the region relative to stone and \mathbf{D}_2 the region relative to mortar. Since \mathbf{D}_1 and \mathbf{D}_2 are the complements of one another, then $\mathbf{D}_1 \cup \mathbf{D}_2 = \mathbf{D}$ and $\mathbf{D}_1 \cap \mathbf{D}_2 = \emptyset$.

For a given realization, the indicator function (or characteristic function) $\chi^i(\mathbf{x})$ for the phase $i = 1, 2$, given $\mathbf{x} \in \mathbf{D}$, is defined by

$$\chi^i(\mathbf{x}) = \begin{cases} 1 & \text{if } \mathbf{x} \in \mathbf{D}_i, \\ 0 & \text{otherwise,} \end{cases} \quad \text{with } \chi^1(\mathbf{x}) + \chi^2(\mathbf{x}) = 1. \quad (1)$$

The probabilistic descriptor of $\chi^i(\mathbf{x})$ is given by the n -point probability function for phase i [Torquato and Stell 1982]

$$S_n^i(\mathbf{x}_1, \mathbf{x}_2, \dots, \mathbf{x}_n) = P\{\chi^i(\mathbf{x}_1) = 1, \chi^i(\mathbf{x}_2) = 1, \dots, \chi^i(\mathbf{x}_n) = 1\}, \quad (2)$$

which gives the probability that n points at positions $\mathbf{x}_1, \mathbf{x}_2, \dots, \mathbf{x}_n$ are found in phase i .

The random medium is strictly statistically homogeneous if there is not a preferred origin in the system so that, for all $n \geq 1$ and all $\mathbf{y} \in \mathbf{D}$

$$S_n^i(\mathbf{x}_1, \mathbf{x}_2, \dots, \mathbf{x}_n) = S_n^i(\mathbf{x}_1 + \mathbf{y}, \mathbf{x}_2 + \mathbf{y}, \dots, \mathbf{x}_n + \mathbf{y}). \quad (3)$$

In particular, the one-point probability function is constant and equal to the volume fraction ϕ_i of the phase i : $S_1^i(\mathbf{x}_1) = \phi_i$.

From this point of view, the masonry has a locally heterogeneous microstructure, but it can be considered homogeneous overall when a sufficiently large portion of it is taken into account. In the following, statistical descriptors up to the second order will be considered so that the masonry wall will be assumed to be a weakly homogeneous random field.

If the random medium is ergodic then the result of averaging over all the realizations of the ensemble is equivalent to that of averaging over the surface for one realization in the infinite-surface limit. In this way probabilistic information can be obtained from a single realization of the infinite medium.

The masonry will be assumed, in the following, to be an ergodic medium. Moreover, it is assumed that the probabilistic characteristics of the medium can be estimated by analyzing a portion of the wall. This portion must be sufficiently large to make it adequately representative of the medium; furthermore this condition permits one to replace the averaging in the infinite-surface limit with the numerical approximation derived from the averaging over the surface of the portion.

3.1. Statistical descriptors of stones and mortar joints. Masonry is, as we noted above, a very distinctive random medium, and we shall therefore introduce statistical descriptors to represent this peculiarity. These descriptors will refer to the type of masonry shown in [Figure 1](#), but they can be applied to a very large number of masonry typologies.

The portion of masonry shown in [Figure 1](#) has been taken as a representative sample of the structure as a whole. Considering, in particular, the construction of the wall in superimposed courses, the random field of masonry was described using a grid that was set up as follows ([Figure 2](#)):

- The rows of the grid are horizontal lines drawn in correspondence with the center points of the stones; rows are indicated by R_j with $j = 1, \dots, N_{Rj}$ ($N_{Rj} = 23$).
- The columns are vertical lines starting from the center points of the stones of R_1 ; columns are indicated by C_j with $j = 1, \dots, N_{Cj}$ ($N_{Cj} = 18$).
- Along the rows, for each course $j = 1, \dots, N_{Rj}$, the widths of the stones $B_{st,k}^j$ $k = 1, 2, \dots$ and the sizes of the mortar joints $B_{m,k}^j$ $k = 1, 2, \dots$ were measured.

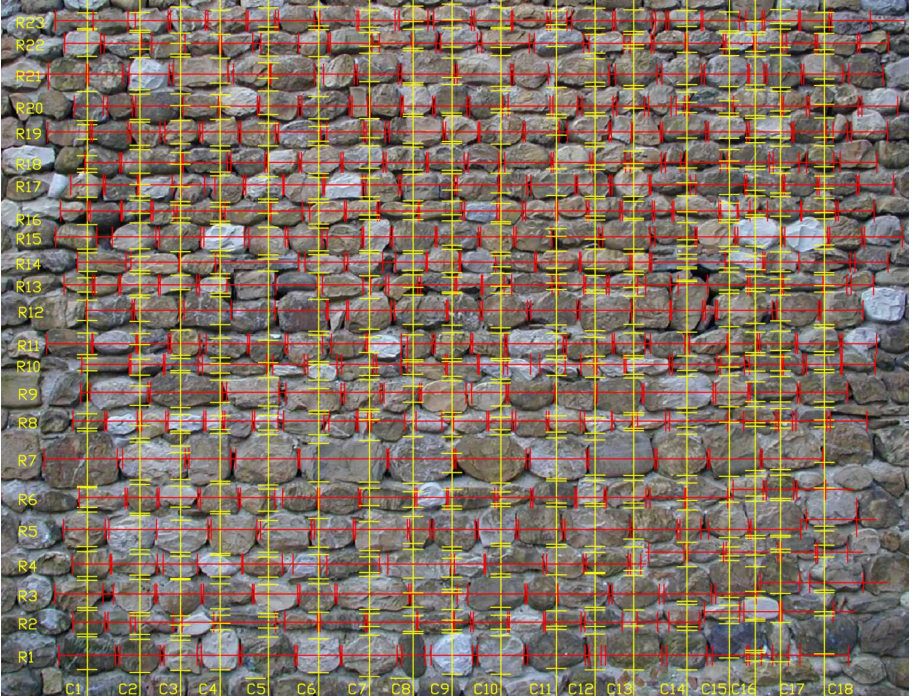


Figure 2. Masonry wall with superimposed orthogonal grid; rows R_j ($j = 1, \dots, N_{Rj}$; $N_{Rj} = 23$) and columns C_j ($j = 1, \dots, N_{Cj}$; $N_{Cj} = 18$).

- The heights of the stones $H_{st,k}^j$ $k = 1, 2, \dots$ and the thicknesses of the mortar joints $H_{m,k}^j$ $k = 1, 2, \dots$ were measured along each column $j = 1, \dots, N_{Cj}$ (note that $H_{m,k}^j$ represents the thickness of the bed joints, but it can, in some cases, indicate the height of the head joint between rows).

A grid rather than image analysis with small pixels was preferred because the former reflects the intrinsically horizontal/vertical structure of the masonry and because the irregularities of the surface would make it extremely difficult to use the pixels in distinguishing mortar from stone.

Considering the previous values the following samples were obtained: $\{B_{st}\}$ and $\{H_{st}\}$ for the widths and heights of the stones, and $\{B_m\}$ and $\{H_m\}$ for the sizes of bed and head mortar joints.

The portion of the wall considered, shown in [Figure 2](#), was sufficiently large (432×341 cm) that the previous samples were assumed to be statistically representative of the geometric characteristics of the inclusions and of the matrix. These samples were therefore taken to be the statistical descriptors of the masonry continuum.

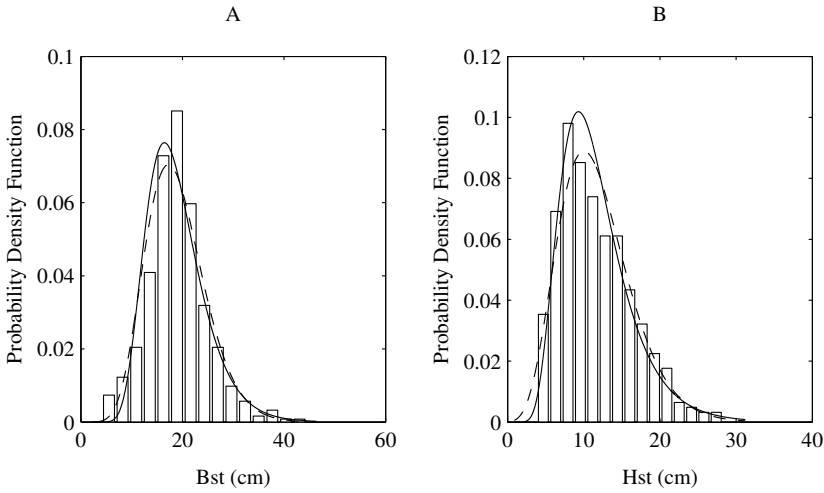


Figure 3. Comparison among the probability density functions of the width of the stones P_{Bst} , the heights of the stones P_{Hst} , the gamma (dashed line), and the log-normal curve (continuous line).

These samples were analyzed to determine their statistical moments up to the second order:

- the mean values of the width and height of the stones: E_{Bst} and E_{Hst} , respectively;
- the mean values of the mortar joint dimensions: E_{Bm} and E_{Hm} , respectively;
- the standard deviation values for the same samples: Σ_{Bst} , Σ_{Hst} , Σ_{Bm} and Σ_{Hm} .

These values are reported in [Table 3](#).

The comparison among the probability density functions of the width of the stones P_{Bst} , the gamma curve, and the log-normal curve are shown in [Figure 3 \(A\)](#). The same comparison for the probability density functions of the height of the stones P_{Hst} is reported in [Figure 3 \(B\)](#). Note that both gamma and log-normal laws are not rejected by the chi-square test.

The probability density functions of the characteristics of the mortar joints P_{Bm} and P_{Hm} are reported in [Figure 4 \(A\)](#) and (B). In these figures the probability density functions are compared only with the log-normal curve, since the gamma law was rejected.

3.2. Statistical descriptors of the masonry wall texture. The previous statistical descriptors give information only about stones and mortar joints. Conversely, the mechanical behavior of a masonry wall is influenced by its texture.

We use the following approach to describe this feature.

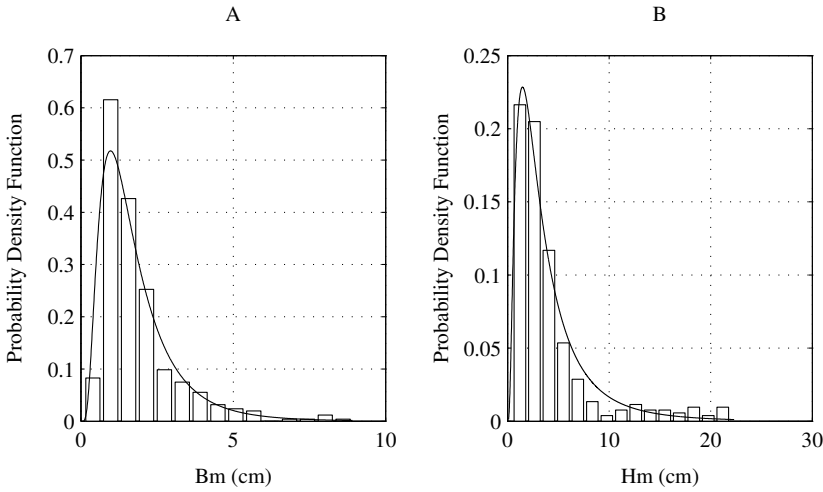


Figure 4. Comparison between the probability density functions of the characteristics of the mortar joints: P_{Bm} and P_{Hm} , and the log-normal curve.

Let $R_j(x)$ be the characteristic function relative to the row R_j $j = 1, \dots, N_{R_j}$: if the point, with abscissa x , belongs to the “stone phase”, the function assumes the value 1; if the point belongs to the “mortar phase”, the function value is 0:

$$R_j(x) = \begin{cases} 1 & x \in \text{stone phase,} \\ 0 & x \in \text{mortar phase,} \end{cases} \tag{4}$$

where $0 \leq x \leq L_{R_j}$ and $L_{R_j} = \sum_k (B_{st,k}^j + B_{m,k}^j)$ is the total length of the row R_j .

Let $C_j(y)$ be the characteristic function relative to the column C_j $j = 1, \dots, N_{C_j}$:

$$C_j(y) = \begin{cases} 1 & y \in \text{stone phase,} \\ 0 & y \in \text{mortar phase,} \end{cases} \tag{5}$$

where $0 \leq y \leq L_{C_j}$ and $L_{C_j} = \sum_k (H_{st,k}^j + H_{m,k}^j)$ is the total length of the column C_j .

In order to estimate the second-order characteristics of $R_j(x)$, the “shifted-area function” (SAF) $A_{R_j,R_j}(\xi)$ was introduced. Given $\xi \in \mathbf{R}$, this function $A_{R_j,R_j}(\xi)$ corresponds to the mean square value of the area below the curve expressing the difference between the shifted function $R_j(x + \xi)$ and the function $R_j(x)$:

$$A_{R_j,R_j}(\xi) = \lim_{\Delta x \rightarrow \infty} \frac{1}{\Delta x} \int_0^{\Delta x} [R_j(x + \xi) - R_j(x)]^2 dx. \tag{6}$$

In the application the integral is replaced by a summation extended on the row.

This function gives immediate information about periodic texture (Figure 5) because it assumes null value for $\xi = 0$ and $\xi = nX$, where $X \in R$ is the period and $n = 1, 2, \dots$ (see Figure 5, where the shifted-area function is normalized to its maximum value).

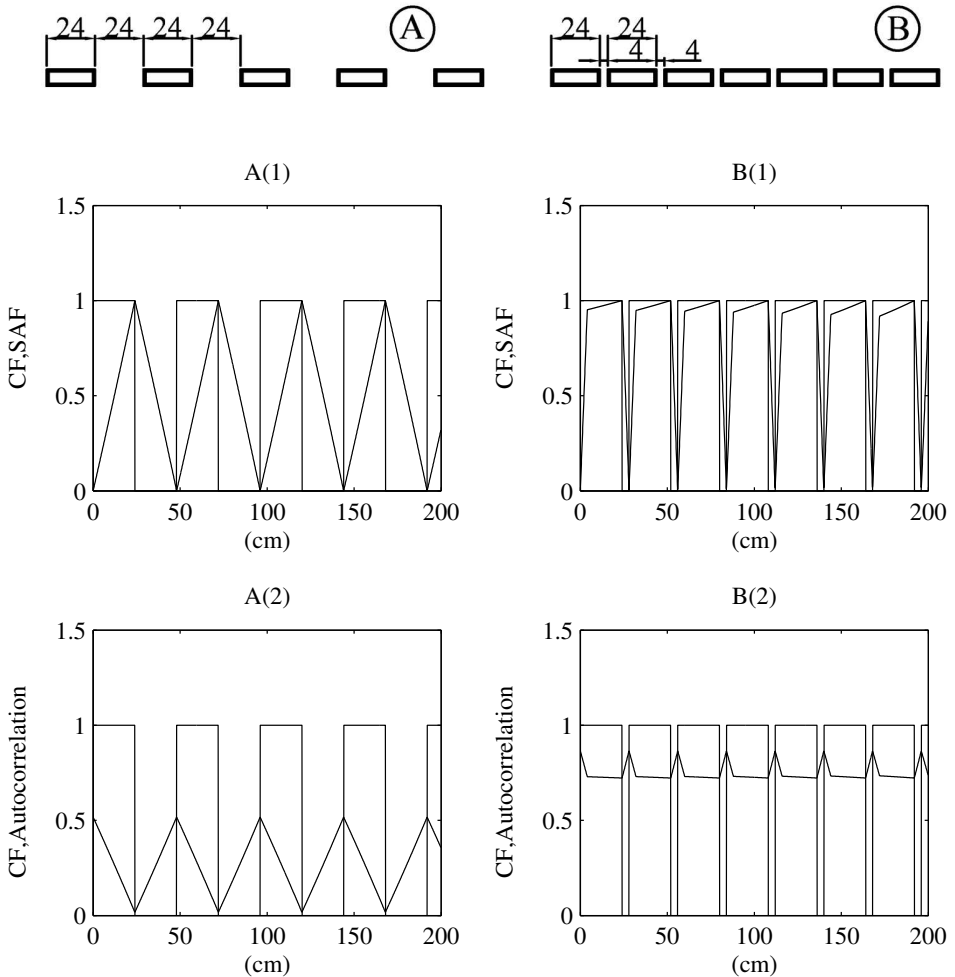


Figure 5. Courses in masonry with different periodic textures (measured in cm). Characteristic functions (CF), normalized shifted-area functions (SAF) (top) and autocorrelation functions (bottom).

Given the ergodicity hypothesis, the shifted-area function $A_{R_j, R_j}(\xi)$ is related to the autocorrelation function $AC_{R_j, R_j}(\xi)$ of $R_j(x)$ by

$$\begin{aligned} A_{R_j, R_j}(\xi) &= \lim_{\Delta x \rightarrow \infty} \frac{1}{\Delta x} \int_0^{\Delta x} [R_j(x + \xi)]^2 dx \\ &\quad - 2 \lim_{\Delta x \rightarrow \infty} \frac{1}{\Delta x} \int_0^{\Delta x} R_j(x + \xi) R_j(x) dx + \lim_{\Delta x \rightarrow \infty} \frac{1}{\Delta x} \int_0^{\Delta x} [R_j(x)]^2 dx \\ &= 2 \lim_{\Delta x \rightarrow \infty} \frac{1}{\Delta x} \int_0^{\Delta x} [R_j(x)]^2 dx - 2AC_{R_j, R_j}(\xi). \end{aligned} \quad (7)$$

We then have

$$AC_{R_j, R_j}(\xi) = \lim_{\Delta x \rightarrow \infty} \frac{1}{\Delta x} \int_0^{\Delta x} R_j(x + \xi) R_j(x) dx = \frac{2E_{R_j}^2 - A_{R_j, R_j}(\xi)}{2}, \quad (8)$$

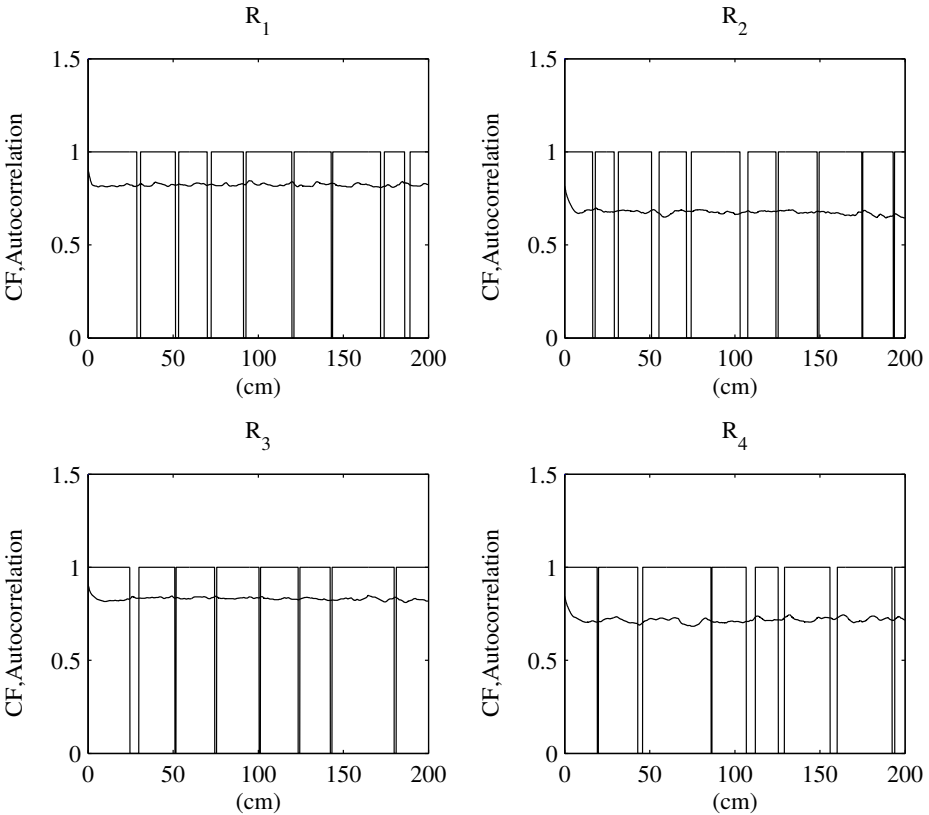


Figure 6. Characteristic functions (CF) and autocorrelation functions relative to the first four rows R_j ($j = 1, \dots, 4$) of the masonry wall in [Figure 2](#).

where

$$E_{R_j}^2 = \lim_{\Delta x \rightarrow \infty} \frac{1}{\Delta x} \int_0^{\Delta x} [R_j(x)]^2 dx \quad (9)$$

is the mean square value of $R_j(x)$.

Given Equation (7), $E_{R_j}^2$ is the ratio of stone to stone plus mortar for the row R_j ; moreover $AC_{R_j, R_j}(\xi) = E_{R_j}^2$ for $\xi = 0$.

The autocorrelation functions for periodic patterns are illustrated in Figure 5.

For the masonry wall in Figure 2, the characteristic functions $R_j(x)$ and the autocorrelation functions $AC_{R_j, R_j}(\xi)$ relative to the first four rows ($j = 1, 2, 3, 4$) are reported in Figure 6.

Figure 7 shows the autocorrelation functions $AC_{R_j, R_j}(\xi)$ for $j = 1, \dots, 11$.

Higher autocorrelation functions are observed in the courses with larger stones (the largest correlation corresponds to the case indicated by (A) in Figure 7 relative to row $R_7(x)$); a weaker correlation is observed in courses with smaller stones (these cases are indicated by (C) in Figure 7).

When we consider the characteristic function $C_j(y)$, we obtain the shifted-area

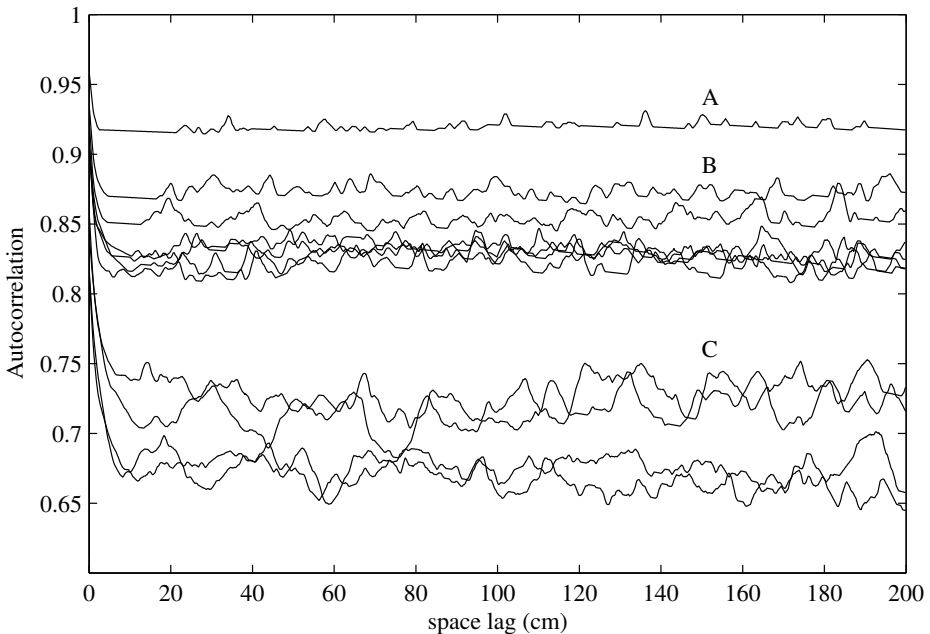


Figure 7. Autocorrelation functions of the first eleven rows R_j ($j = 1, \dots, 11$) of the masonry wall in Figure 2.

function:

$$A_{C_j, C_j}(\eta) = \lim_{\Delta y \rightarrow \infty} \frac{1}{\Delta y} \int_0^{\Delta y} [C_j(y + \eta) - C_j(y)]^2 dy, \tag{10}$$

$$AC_{C_j, C_j}(\eta) = \lim_{\Delta y \rightarrow \infty} \frac{1}{\Delta y} \int_0^{\Delta y} C_j(y + \eta)C_j(y) dy = \frac{2E_{C_j}^2 - A_{C_j, C_j}(\eta)}{2}, \tag{11}$$

$$E_{C_j}^2 = \lim_{\Delta y \rightarrow \infty} \frac{1}{\Delta y} \int_0^{\Delta y} [C_j(y)]^2 dy. \tag{12}$$

The characteristic functions $C_j(x)$ and the autocorrelation functions $AC_{C_j, C_j}(\eta)$ relative to the first four columns ($j = 1, 2, 3, 4$) of the masonry wall are reported in [Figure 8](#).

[Figure 9](#) shows the autocorrelation functions $AC_{C_j, C_j}(\eta)$ for $j = 1, \dots, 11$.

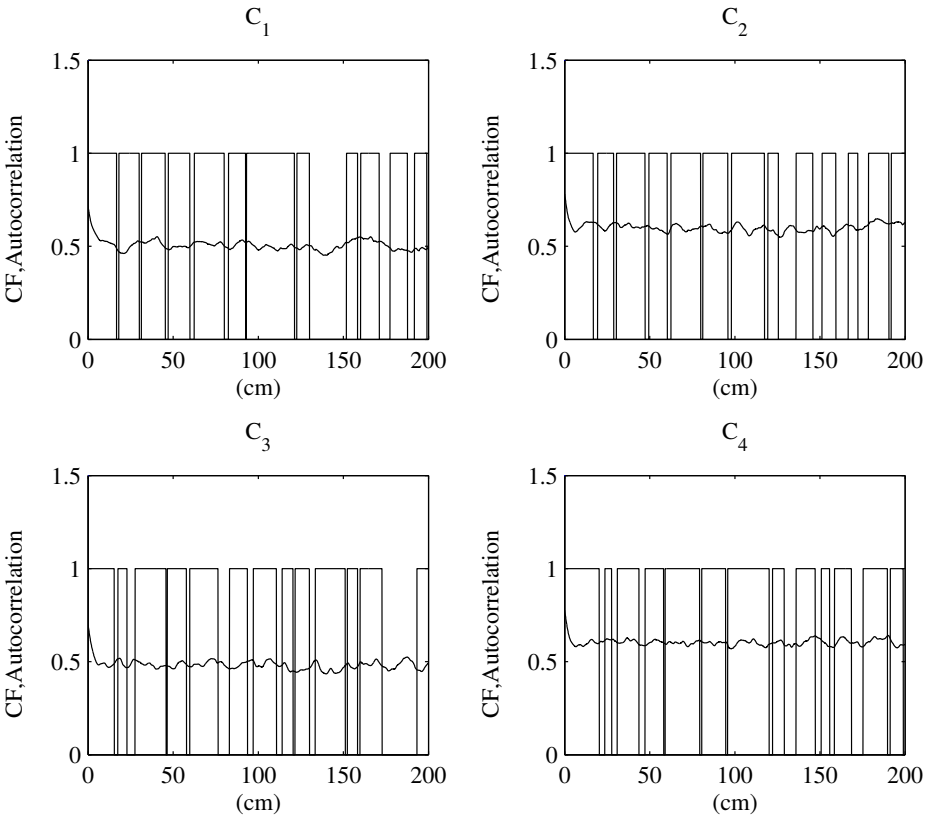


Figure 8. Characteristic functions (CF) and the autocorrelation functions relative to the first four columns C_j ($j = 1, \dots, 4$) of the masonry wall in [Figure 2](#).

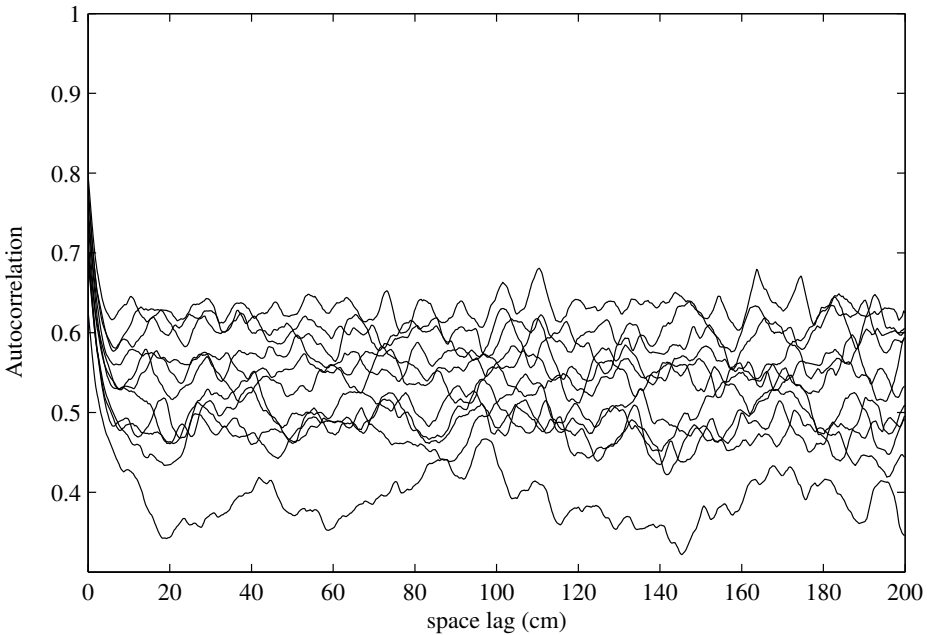


Figure 9. Autocorrelation functions of the first eleven columns C_j , $j = 1, \dots, 11$ of the masonry wall in [Figure 2](#).

These functions exhibit analogous behaviors and show a weaker correlation than that of the [Figure 7](#) courses. This is as we expected; in fact, good building practice dictates the use of stones with similar dimensions (width and height) within a single row. Moreover, the head-joint thicknesses are limited, and, conversely, within columns stones differ in height and bed-mortar joints are thicker. These conditions imply that the correlation is stronger within the courses than within the columns. The autocorrelation functions relative to the rows $AC_{R_j, R_j}(\xi)$ and to the columns $AC_{C_j, C_j}(\eta)$ are taken to be the statistical descriptors of the masonry's texture.

The autocorrelation functions $AC_{R_j, R_j}(\xi)$ and $AC_{C_j, C_j}(\eta)$ were used to check the correctness of the weakly homogeneous random field hypothesis. In fact, using different origins to compute the space lags ξ and η showed that the differences among these functions were very limited, both for the rows and for the columns.

Further information about texture can be evinced by:

- the cross-correlation function $CC_{R_j, R_k}(\xi)$ between rows:

$$\begin{aligned}
 CC_{R_j, R_k}(\xi) &= \lim_{\Delta x \rightarrow \infty} \frac{1}{\Delta x} \int_0^{\Delta x} R_j(x + \xi) R_k(x) dx \\
 &= \frac{E_{R_j}^2 + E_{R_k}^2 - A_{R_j, R_k}(\xi)}{2}, \tag{13}
 \end{aligned}$$

where

$$A_{R_j, R_k}(\xi) = \lim_{\Delta x \rightarrow \infty} \frac{1}{\Delta x} \int_0^{\Delta x} [R_j(x + \xi) - R_k(x)]^2 dx; \quad (14)$$

– the cross-correlation function $CC_{C_j, C_k}(\xi)$ between columns:

$$\begin{aligned} CC_{C_j, C_k}(\eta) &= \lim_{\Delta y \rightarrow \infty} \frac{1}{\Delta y} \int_0^{\Delta y} C_j(y + \eta) C_k(y) dy \\ &= \frac{E_{C_j}^2 + E_{C_k}^2 - A_{C_j, C_k}(\eta)}{2}, \end{aligned} \quad (15)$$

where

$$A_{C_j, C_k}(\eta) = \lim_{\Delta y \rightarrow \infty} \frac{1}{\Delta y} \int_0^{\Delta y} [C_j(y + \eta) - C_k(y)]^2 dy; \quad (16)$$

– the cross-correlation function $CC_{R_j, C_k}(\xi)$ between rows and columns:

$$\begin{aligned} CC_{R_j, C_k}(\xi) &= \lim_{\Delta x \rightarrow \infty} \frac{1}{\Delta x} \int_0^{\Delta x} R_j(x + \xi) C_k(y) dx \\ &= \frac{E_{R_j}^2 + E_{C_k}^2 - A_{R_j, C_k}(\xi)}{2}, \end{aligned} \quad (17)$$

where

$$A_{R_j, C_k}(\xi) = \lim_{\Delta x \rightarrow \infty} \frac{1}{\Delta x} \int_0^{\Delta x} [R_j(x + \xi) - C_k(y)]^2 dx. \quad (18)$$

The column pairs and row-column pairs show patterns that are less strongly cross-correlated than those of the row pairs (Figure 10).

4. Convergence criteria

In order to determine the elastic moduli of the homogeneous continuum equivalent to the masonry it is necessary to estimate the representative volume element. Following [Cluni and Gusella 2004], this estimate can be performed by using the finite-size test-window method. Here this method is improved, however, by coupling the classical mechanical convergence criterion with a probabilistic convergence criterion which considers the statistical descriptors introduced above.

Consider a “material window” with a representative size L placed at any given point in the wall. This window plays the role of the L -Volume Element (VE_L).

Let $T_{ij,L}^e$ (\mathbf{T}_L^e in matrix notation) indicate the elastic stiffness components obtained under essential boundary conditions applied to an VE_L , and let $S_{ij,L}^n$ (\mathbf{S}_L^n) indicate the elastic compliance components obtained under natural conditions. The $T_{ij,L}^n$ natural elastic stiffness components are obtained by inversion: $\mathbf{T}_L^n = [\mathbf{S}_L^n]^{-1}$.

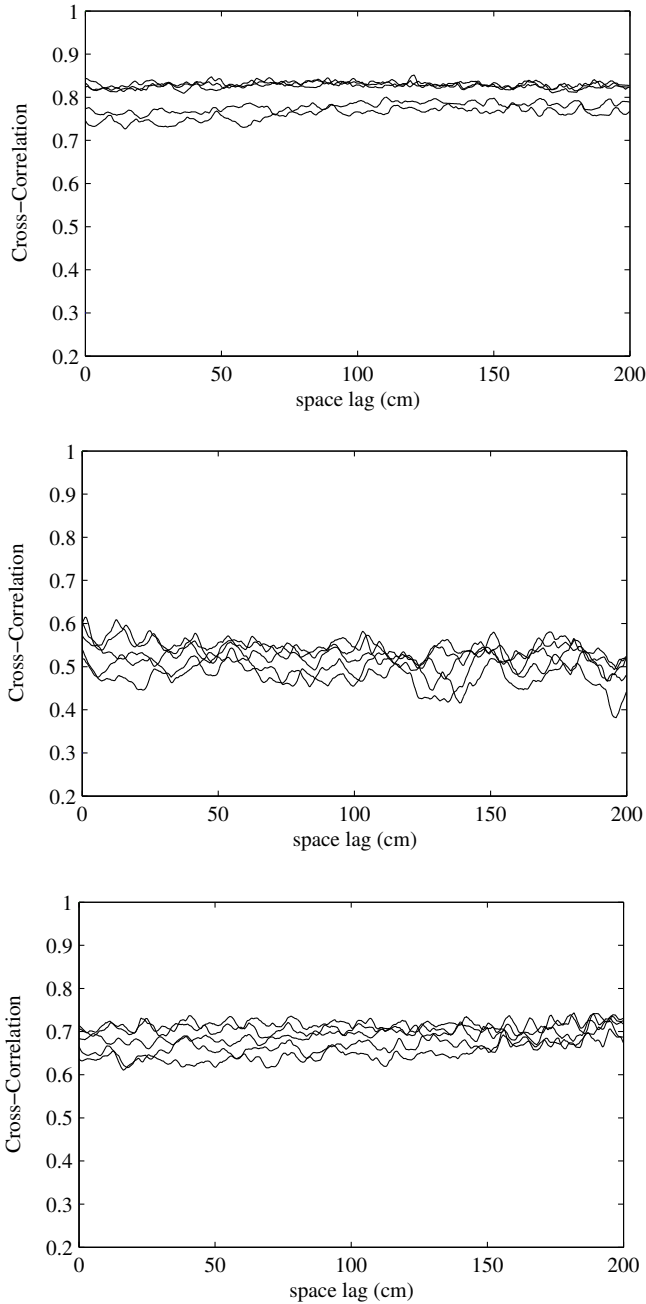


Figure 10. Cross-correlation functions between rows and columns for the wall in Figure 2. Top: rows R_1 and R_j ($j = 2, \dots, 6$); middle: columns C_1 and C_j ($j = 2, \dots, 6$); bottom: row R_1 and columns C_j ($j = 1, \dots, 5$).

We consider the statistical descriptors relative to the inclusions and texture of the VE_L :

- the samples of stone sizes $\{B_{st}^L\}$ and $\{H_{st}^L\}$ with mean values, standard deviations, and probability density functions: $E_{B_{st}}^L$, $E_{H_{st}}^L$, $\Sigma_{B_{st}}^L$, $\Sigma_{H_{st}}^L$, $P_{B_{st}}^L$, $P_{H_{st}}^L$, respectively;
- the samples of mortar joint sizes $\{B_m^L\}$ and $\{H_m^L\}$, with mean values, standard deviations, and probability density function $E_{B_m}^L$, $E_{H_m}^L$, $\Sigma_{B_m}^L$, $\Sigma_{H_m}^L$, $P_{B_m}^L$, $P_{H_m}^L$, respectively;
- the autocorrelation functions relative to the rows $AC_{R_j, R_j}^L(\xi)$ and the columns $AC_{C_j, C_j}^L(\eta)$.

Consider increasing the size of the material window

$$L_k \quad k = 1, \dots, i, j, \dots N \quad (j > i \rightarrow L_j > L_i)$$

thus obtaining the sequence VE_{L_k} .

In order to check that the larger window $VE_{\hat{L}}$, with $\hat{L} = L_N$, is an adequate estimate of the representative volume element, the following *mechanical convergence criterion* can be utilized: Given $\Delta c \in R^+$, the sequence VE_{L_k} converges to the representative volume element when the differences between the natural and essential elastic stiffness of the larger material window $VE_{\hat{L}}$ are limited:

$$\max_{ij} \left| \frac{T_{ij, \hat{L}}^e - T_{ij, \hat{L}}^n}{T_{ij}^1} \right| \leq \Delta c, \quad (19)$$

where

$$T_{ij}^1 = |T_{ij, L_1}^e - T_{ij, L_1}^n|. \quad (20)$$

The exclusively mechanical approach can, nonetheless, introduce an incorrect estimate; in fact Δc is an arbitrary value and the convergence is not uniform (see the following application on the masonry wall in [Figure 1](#)).

In order to overcome this limitation the following *probabilistic convergence criterion* can be used: The sequence VE_{L_k} converges to the representative volume element when the statistical descriptors relative to the elements and the texture of the larger material window $VE_{\hat{L}}$ comply with the statistical descriptors of the random field model relative to the masonry wall as a whole. In other words, the material window $VE_{\hat{L}}$ must be *statistically similar* to the random medium model of the masonry as obtained by analyzing the entire wall.

With regard to the statistical descriptors introduced above, the similarity in stone and mortar joint characteristics is checked by minimizing the differences among

mean values, standard deviations, and probability density functions:

$$\left| \Sigma_{\Pi j} - \Sigma_{\hat{L}_{\Pi j}} \right| \leq \Delta c_{\Sigma_{\Pi j}}, \quad (21)$$

$$\int \left| P_{\Pi j} - P_{\hat{L}_{\Pi j}} \right| d\Pi j \leq \Delta c_{P_{\Pi j}}, \quad (22)$$

where $\Pi = B, H$ and $j = st, m$.

Similarity in texture is checked by minimizing the differences among correlation functions. Let $\bar{A}C_{RR}(\xi)$ be the mean autocorrelation function obtained by averaging, for any space lag ξ , the autocorrelation function of the rows of the masonry wall; let $\bar{A}C_{C,C}(\eta)$ be the mean autocorrelation function relative to the columns. Let $\bar{A}C_{R,R}^{\hat{L}}(\xi)$ and $\bar{A}C_{C,C}^{\hat{L}}(\eta)$ be the same quantities relative to the rows and columns of the material window. The similarity is then checked by:

$$\int \left| \bar{A}C_{Rj,Rj}(\xi) - \bar{A}C_{Rj,Rj}^{\hat{L}}(\xi) \right| d\xi \leq \Delta c_{Rj}, \quad (23)$$

$$\int \left| \bar{A}C_{Cj,Cj}(\eta) - \bar{A}C_{Cj,Cj}^{\hat{L}}(\eta) \right| d\eta \leq \Delta c_{Cj}. \quad (24)$$

If these mechanical and probabilistic convergence criteria are met, then the material window $VE_{\hat{L}}$ is an adequate estimate of the *statistically equivalent representative volume element*. In this case the elastic stiffness components $T_{ij}^{\text{hom}} = T_{ij}^{\text{RVE}}$ of the equivalent homogeneous continuum can be estimated by $T_{ij,\hat{L}}^*$:

$$T_{ij}^{\text{hom}} = T_{ij}^{\text{RVE}} = T_{ij,\hat{L}}^* = \frac{T_{ij,\hat{L}}^e + T_{ij,\hat{L}}^n}{2}. \quad (25)$$

We mention that the linear properties of random composites can be accurately estimated using volumes subjected to periodic boundary conditions. The periodic boundary conditions give an estimation of the effective elastic moduli which are intermediate between those deriving from displacement and those from traction boundary conditions, as demonstrated numerically by [Terada et al. \[2000\]](#) and theoretically by [Sab and B. \[2005\]](#). These conditions could be used to improve the approach proposed in the present paper, however, as will be highlighted in the numerical application, the difference between essential and natural evaluations of the elastic moduli decrease very quickly as L increases.

5. Application

The previous method has been applied in estimating the elastic stiffness components of the homogeneous continuum equivalent to the masonry wall in [Figure 1](#).

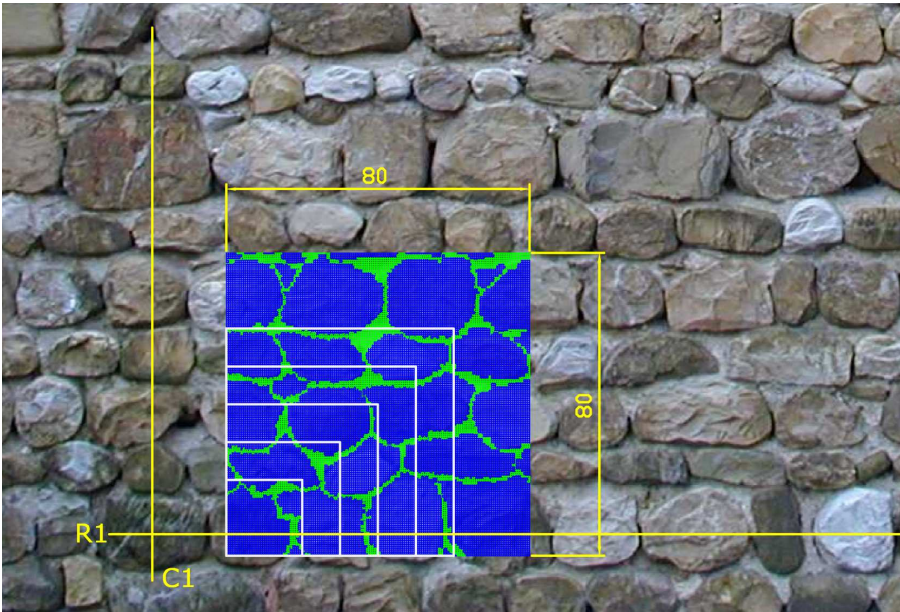


Figure 11. Square material window with $L = 80$ cm and finite element model.

A sequence of square material windows of size L was located in the bottom-left portion. Given the ergodicity hypothesis, the position of the test-windows is arbitrary. The 80 cm window is shown, as an example, in Figure 11.

These windows, which contain both of the composite phases, were modeled by the finite element method using membrane elements measuring 5×5 mm (these finite elements were defined by superimposing a 5×5 mm grid onto the photograph). The mechanical properties of stone and mortar were assumed to be deterministic and are reported in Table 1.

| Phase | Material | Young's module E | Poisson's coefficient ν | T_{11} (MPa) | T_{12} (MPa) | T_{22} (MPa) | T_{33} (MPa) |
|-------|----------|-----------------------|--------------------------------|-------------------|-------------------|-------------------|-------------------|
| 1 | Stone | 12500 | 0.20 | 13021 | 2604 | 13021 | 10417 |
| 2 | Mortar | 1200 | 0.30 | 1319 | 396 | 1319 | 923 |

Table 1. Mechanical properties of the masonry phases: stone and mortar.

5.1. Mechanical convergence. Two types of boundary conditions were applied to the material windows:

(a) *Essential*, in terms of displacements u_i (Dirichlet, displacement-controlled),

$$u_i = \varepsilon_{ij}^0 x_j, \quad (26)$$

where ε_{ij}^0 are constant strains and x_j are point coordinates, or

(b) *Natural*, in terms of tractions t_i (Neumann, or stress-controlled),

$$t_i = \sigma_{ij}^0 n_j, \quad (27)$$

where σ_{ij}^0 are constant stresses and n_j are the components of the unit vector outward from the boundary. The average values of the strain in condition (a) are $\bar{\varepsilon}_{ij} = \varepsilon_{ij}^0$, while the average values of the stress in condition (b) are $\bar{\sigma}_{ij} = \sigma_{ij}^0$, where

$$\bar{\varepsilon}_{ij} = \frac{1}{V} \int_V \varepsilon_{ij} dV \quad \bar{\sigma}_{ij} = \frac{1}{V} \int_V \sigma_{ij} dV. \quad (28)$$

According to Hill [1963], when the volume considered is the representative volume element, then the relation between average stress and strain is the same for both types of boundary conditions (a) and (b).

The masonry is composed of two phases, so that:

$$\bar{\sigma}_{ij} = c_1 \bar{\sigma}_{ij}^{(1)} + c_2 \bar{\sigma}_{ij}^{(2)} = c_1 T_{ijkl}^{(1)} \bar{\varepsilon}_{kl}^{(1)} + c_2 T_{ijkl}^{(2)} \bar{\varepsilon}_{kl}^{(2)}, \quad (29)$$

$$\bar{\varepsilon}_{ij} = c_1 \bar{\varepsilon}_{ij}^{(1)} + c_2 \bar{\varepsilon}_{ij}^{(2)} = c_1 S_{ijkl}^{(1)} \bar{\sigma}_{kl}^{(1)} + c_2 S_{ijkl}^{(2)} \bar{\sigma}_{kl}^{(2)}, \quad (30)$$

where c_1 and c_2 are the fractional concentrations by volume ($c_1 + c_2 = 1$), $T_{ijkl}^{(1)}$ and $T_{ijkl}^{(2)}$ are the elastic stiffness constants, and $S_{ijkl}^{(1)}$ and $S_{ijkl}^{(2)}$ are the elastic compliances of the two phases.

Combining the previous equation we obtain:

$$T_{ijkl}^e \varepsilon_{kl}^0 = T_{ijkl}^{(1)} (\varepsilon_{kl}^0 - c_2 \bar{\varepsilon}_{kl}^{(2)}) + c_2 T_{ijkl}^{(2)} \bar{\varepsilon}_{kl}^{(2)} = T_{ijkl}^{(1)} \varepsilon_{kl}^0 + c_2 (T_{ijkl}^{(2)} - T_{ijkl}^{(1)}) \bar{\varepsilon}_{kl}^{(2)}, \quad (31)$$

$$S_{ijkl}^n \sigma_{kl}^0 = S_{ijkl}^{(1)} (\sigma_{kl}^0 - c_2 \bar{\sigma}_{kl}^{(2)}) + c_2 S_{ijkl}^{(2)} \bar{\sigma}_{kl}^{(2)} = S_{ijkl}^{(1)} \sigma_{kl}^0 + c_2 (S_{ijkl}^{(2)} - S_{ijkl}^{(1)}) \bar{\sigma}_{kl}^{(2)}, \quad (32)$$

where T_{ijkl}^e are the stiffness components under essential conditions and S_{ijkl}^n are the compliance components under natural conditions.

Applying displacement boundary conditions such that $\boldsymbol{\varepsilon}^0 = \mathbf{I}^{mn}$ (\mathbf{I}^{mn} is the symmetrical matrix with all its components set to 0, except the component mn , which is set to 1) it becomes possible to determine the columns of the stiffness matrix \mathbf{T}^e .

Applying traction boundary conditions such that $\boldsymbol{\sigma}^0 = \mathbf{I}^{mn}$, it becomes possible to determine the columns of the compliance matrix \mathbf{S}^n . The stiffness matrix relative to natural conditions is obtained from $\mathbf{T}^n = [\mathbf{S}^n]^{-1}$.

We adopted an orthotropic equivalent continuum:

$$\begin{pmatrix} \sigma_{11} \\ \sigma_{22} \\ \tau_{12} \end{pmatrix} = \begin{bmatrix} T_{11} & T_{12} & T_{13} \\ T_{21} & T_{22} & T_{23} \\ T_{31} & T_{32} & T_{33} \end{bmatrix} \begin{pmatrix} \varepsilon_{11} \\ \varepsilon_{22} \\ \gamma_{12} \end{pmatrix} = \begin{bmatrix} 2G_{11} + \lambda & \lambda & 0 \\ \lambda & 2G_{22} + \lambda & 0 \\ 0 & 0 & G_{12} \end{bmatrix} \begin{pmatrix} \varepsilon_{11} \\ \varepsilon_{22} \\ \gamma_{12} \end{pmatrix}, \quad (33)$$

$$\begin{pmatrix} \varepsilon_{11} \\ \varepsilon_{22} \\ \gamma_{12} \end{pmatrix} = \begin{bmatrix} S_{11} & S_{12} & S_{13} \\ S_{21} & S_{22} & S_{23} \\ S_{31} & S_{32} & S_{33} \end{bmatrix} \begin{pmatrix} \sigma_{11} \\ \sigma_{22} \\ \tau_{12} \end{pmatrix} = \begin{bmatrix} 1/E_{11} & -\nu_{12}/E_{22} & 0 \\ -\nu_{21}/E_{11} & 1/E_{22} & 0 \\ 0 & 0 & 1/G_{12} \end{bmatrix} \begin{pmatrix} \sigma_{11} \\ \sigma_{22} \\ \tau_{12} \end{pmatrix}, \quad (34)$$

where $1 \equiv x$, $2 \equiv y$, $T_{ij} = T_{ji} \leftrightarrow S_{ij} = S_{ji}$, G_{ij} , λ are Lamé's constants, E_{ij} and ν_{ij} are Young's constants and Poisson's coefficients, respectively:

$$\begin{aligned} E_{11} &= \frac{(2G_{11} + \lambda)(2G_{22} + \lambda) - \lambda^2}{2G_{22} + \lambda}; & E_{22} &= \frac{(2G_{11} + \lambda)(2G_{22} + \lambda) - \lambda^2}{2G_{11} + \lambda}; \\ \nu_{21} &= \frac{\lambda}{2G_{11} + \lambda}; & \nu_{12} &= \frac{\lambda}{2G_{22} + \lambda}; & \frac{\nu_{12}}{E_{22}} &= \frac{\nu_{21}}{E_{11}}. \end{aligned} \quad (35)$$

In order to determine the three columns of the essential stiffness matrix, the following strains and boundary displacements were applied (for details see [Cluni and Gusella 2004]):

$$\begin{aligned} \boldsymbol{\varepsilon}_1^0 &= \begin{pmatrix} 1 \\ 0 \\ 0 \end{pmatrix} \leftrightarrow \begin{pmatrix} u_1 \\ u_2 \end{pmatrix} = \begin{pmatrix} x \\ 0 \end{pmatrix}, & \boldsymbol{\varepsilon}_2^0 &= \begin{pmatrix} 0 \\ 1 \\ 0 \end{pmatrix} \leftrightarrow \begin{pmatrix} u_1 \\ u_2 \end{pmatrix} = \begin{pmatrix} 0 \\ y \end{pmatrix}, \\ \boldsymbol{\varepsilon}_3^0 &= \begin{pmatrix} 0 \\ 0 \\ 1 \end{pmatrix} \leftrightarrow \begin{pmatrix} u_1 \\ u_2 \end{pmatrix} = \begin{pmatrix} x \\ y \end{pmatrix}. \end{aligned} \quad (36)$$

In order to determine the three columns of the natural compliance matrix, the following stresses and boundary tractions were applied

$$\begin{aligned} \boldsymbol{\sigma}_1^0 &= \begin{pmatrix} 1 \\ 0 \\ 0 \end{pmatrix} \leftrightarrow \begin{pmatrix} t_1 \\ t_2 \end{pmatrix} = \begin{pmatrix} 1 \\ 0 \end{pmatrix}, & \boldsymbol{\sigma}_2^0 &= \begin{pmatrix} 0 \\ 1 \\ 0 \end{pmatrix} \leftrightarrow \begin{pmatrix} t_1 \\ t_2 \end{pmatrix} = \begin{pmatrix} 0 \\ 1 \end{pmatrix}, \\ \boldsymbol{\sigma}_3^0 &= \begin{pmatrix} 0 \\ 0 \\ 1 \end{pmatrix} \leftrightarrow \begin{pmatrix} t_1 \\ t_2 \end{pmatrix} = \begin{pmatrix} 1 \\ 1 \end{pmatrix}. \end{aligned} \quad (37)$$

Since an L -size window is used, the essential stiffness is designated \mathbf{T}_L^e and the natural stiffness is designated \mathbf{T}_L^n .

Introducing

$$T_{ij,L}^* = \frac{T_{ij,L}^e + T_{ij,L}^n}{2} \quad [T_L^* = (T_L^e + T_L^n)/2], \quad (38)$$

we have [Huet 1990; Sab 1992; Ostoja-Starzewski 1998]:

$$T_L^R \leq T_L^n \leq T_L^* \leq T_L^e \leq T_L^V, \quad (39)$$

where T_L^R and T_L^V are the Reuss and Voigt bounds, respectively ($A \leq B$ means that $v^T A v \leq v^T B v$ for all $v \neq 0$).

As the size L of the window increases, the difference between T_L^e and T_L^n decreases. As L goes to infinity, the VE_L converges with the representative volume element, and T_L^* converges with the stiffness matrix of the nonrandom equivalent homogeneous continuum $T^{\text{RVE}} = T^{\text{hom}}$ [Sab 1992]

$$\lim_{L \rightarrow \infty} T_L^* = T^{\text{RVE}} = T^{\text{hom}}. \quad (40)$$

In effective applications, the window has a finite size which increases, giving the sequence: L_k $k = 1, \dots, N$ with $i > j \rightarrow L_j > L_i$. Applying the mechanical convergence criterion introduced above the material window with $\hat{L} = L_n$ is an adequate estimate of the representative volume element when the equation (3) is verified:

$$\max_{ij} \left| \frac{T_{ij,\hat{L}}^e - T_{ij,\hat{L}}^n}{T_{ij}^1} \right| \leq \Delta c, \quad (41)$$

where $T_{ij}^1 = |T_{ij,L_1}^e - T_{ij,L_1}^n|$ and $\Delta c \in R^+$ is a fixed admissible error.

In the present application the size L was increased from 20 cm to 130 cm (the 130 cm window is shown in Figure 12).

At first, the numerical results confirmed the hypothesis in Equations (33) and (34); in fact the stiffness components T_{i3} $i = 1, 2$ and the compliance components S_{i3} $i = 1, 2$ were negligible with respect to the others. Table 2 reports the Young's moduli and Lamé constants relative to essential and natural conditions. The convergence of these characteristics is shown in Figure 13. Poisson's coefficients converge very quickly (for the window with $L = 130$ cm: $\nu_{21} = 0.199$, $\nu_{12} = 0.203$ for essential conditions, and $\nu_{21} = 0.178$, $\nu_{12} = 0.180$ for natural conditions).

5.2. Probabilistic convergence. The previous mechanical convergence does not permit us to state with adequate reliability that the test-window is a good approximation of the representative volume element. Differences between essential and natural evaluations of the elastic moduli decrease very quickly as L increases. The convergence could be accelerated by averaging over several samples of the same

| L (cm) | Essential Boundary Conditions | | | Natural Boundary Conditions | | |
|-------------|-------------------------------|----------------|----------------|-----------------------------|----------------|----------------|
| | E_{11} (MPa) | E_{22} (MPa) | G_{12} (MPa) | E_{11} (MPa) | E_{22} (MPa) | G_{12} (MPa) |
| 20 | 7807.03 | 7698.80 | 3271.50 | 6408.04 | 6338.20 | 2487.00 |
| 30 | 7890.46 | 7752.42 | 3162.00 | 7086.51 | 6665.78 | 2710.50 |
| 40 | 7929.02 | 7852.14 | 3255.50 | 7214.07 | 7290.57 | 2883.00 |
| 50 | 7894.35 | 7290.79 | 3049.50 | 7401.59 | 6709.97 | 2724.00 |
| 60 | 7840.72 | 7079.91 | 2917.51 | 7504.52 | 6584.28 | 2625.44 |
| 80 | 7937.80 | 7055.86 | 2893.87 | 7658.00 | 6601.37 | 2655.77 |
| 100 | 7813.77 | 6929.10 | 2816.60 | 7543.66 | 6677.43 | 2657.16 |
| 120 | 8095.70 | 7290.24 | 2932.05 | 7879.92 | 7058.18 | 2784.91 |
| 130 | 8143.23 | 7282.57 | 2940.33 | 7958.80 | 7046.80 | 2801.83 |

Table 2. Mechanical characteristics obtained under essential and natural boundary conditions as L , the side of the square window, increases.

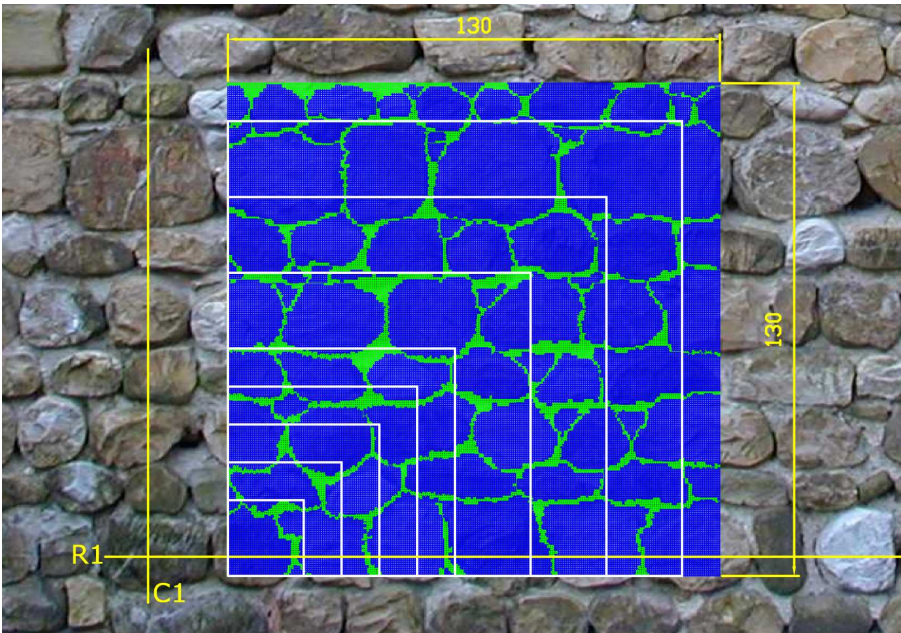


Figure 12. Square material window with $L = 130$ cm and finite element model.

size, as noted in [Cluni and Gusella 2004]; the averaging over samples with different sizes is not appropriate because these samples have different and unknown statistical weights.

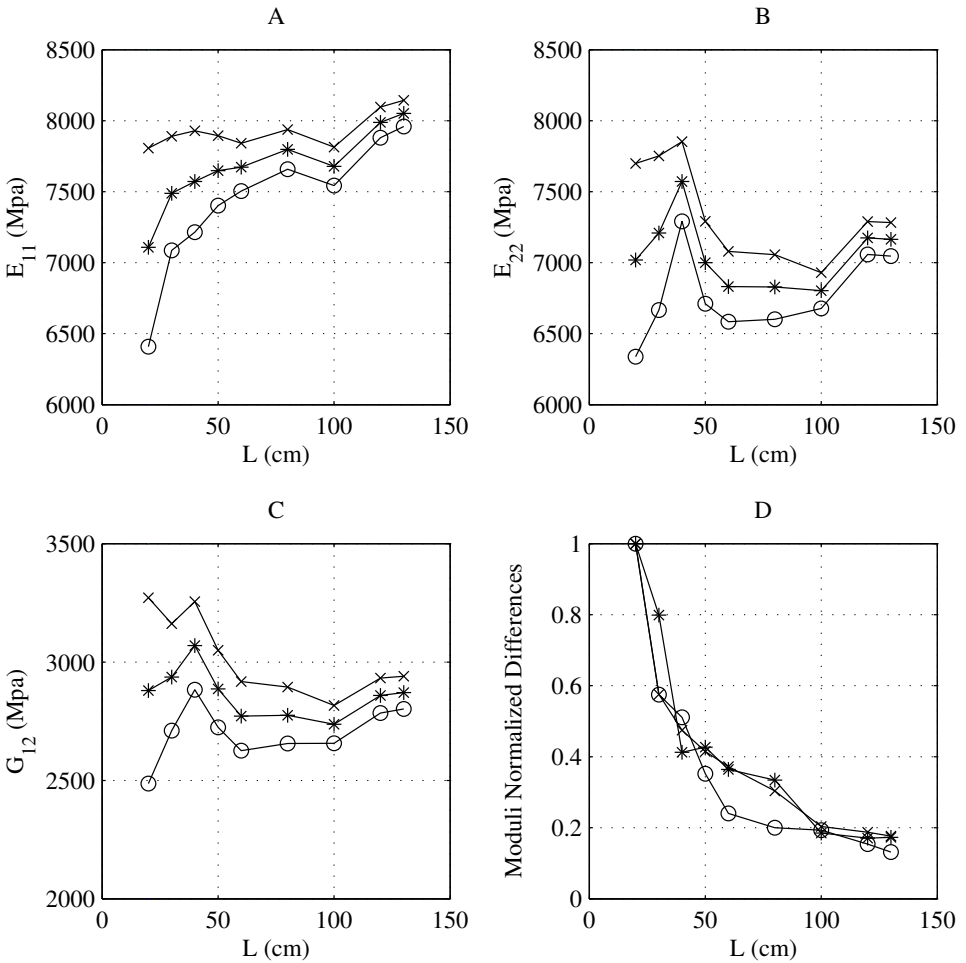


Figure 13. (A), (B) and (C): behavior of the mechanical properties of the test-window as L increases: “ \times ” essential, “ \circ ” natural, “ $*$ ” mean value; (D) normalized differences between essential and natural evaluations for E_{11} , E_{22} , and G_{12} .

Even with a single 80 cm window, the differences between essential and natural moduli are limited. However, for the 130 cm window these differences are quite similar to those noted above, whereas the values of essential and natural elastic moduli and their mean values are significantly different from those of the 80 cm window (Figure 13 (A)–(C)).

This discrepancy can be explained by observing that the 80 cm window does not adequately represent the masonry wall because it does not contain a representative

| | Bst | | Hst | | Bm | | Hm | |
|---------------|---------------------------|-------------------------------|---------------------------|-------------------------------|-------------------------|------------------------------|-------------------------|------------------------------|
| Entire wall | E_{Bst} 18.87 | Σ_{Bst} 5.86 | E_{Hst} 11.69 | Σ_{Hst} 4.73 | E_{Bm} 4.20 | Σ_{Bm} 4.22 | E_{Hm} 1.81 | Σ_{Hm} 1.29 |
| VE_L | E_{Bst}^L | Σ_{Bst}^L | E_{Hst}^L | Σ_{Hst}^L | E_{Bm}^L | Σ_{Bm}^L | E_{Hm}^L | Σ_{Hm}^L |
| 80 × 80 | 21.61 | 3.45 | 13.34 | 5.02 | 2.79 | 1.56 | 2.06 | 1.62 |
| 130 × 130 | 19.90 | 5.57 | 12.75 | 4.98 | 3.70 | 3.48 | 1.83 | 1.25 |

Table 3. Mean E and standard deviation Σ of the width and the height of the stones, head and bed mortar joints, for the portion of wall shown in [Figure 2](#) and for the material windows with $L = 80$ cm ([Figure 11](#)) and $L = 130$ cm ([Figure 12](#)).

sample of stones: for example, the course with very large stones (row R_7 in [Figure 2](#)) is not taken into account.

It should, therefore, be noted that as the size of the test-window increases, the differences between the essential and natural components decrease, but the convergence to the equivalent homogeneous continuum components is not uniform. In order to overcome this limitation the probabilistic convergence criterion introduced above was applied, taking into account Equations (21), (22), (23) and (25).

Excluding windows with $L < 60$ cm, because the number of stones and joints was too small, the means and standard deviations of the sample relative to the stone and mortar joint sizes were compared with those of the entire wall (see [Table 3](#)).

Moreover, for $L \geq 80$ cm, the probability density functions of these samples were compared with those of the entire wall. Comparisons relative to the width and height of the stones in the windows with $L = 80$ cm, the window with $L = 130$ cm, and the wall as a whole, are shown in [Figure 14](#). Comparisons relative to the mortar joint sizes are shown in [Figure 15](#).

The window with $L = 130$ cm is adequately representative of the statistical distribution of stones and mortar joints in the masonry (only the sample of the bed joint thickness should be improved). In fact, the differences ([Table 3](#)) in statistical moments (mean and standard deviation) and in probability density functions ([Figures 14](#) and [15](#)) between the 130 cm window and the entire wall were found to be sufficiently limited.

Moreover, it is necessary to check that the pattern of the window is representative of the entire wall. This was done by analyzing the autocorrelation functions of the rows and columns. The results relative to the 130 cm window are shown in [Figure 16](#). These functions match those relative to the entire wall ([Figure 7](#) and [Figure 9](#)).

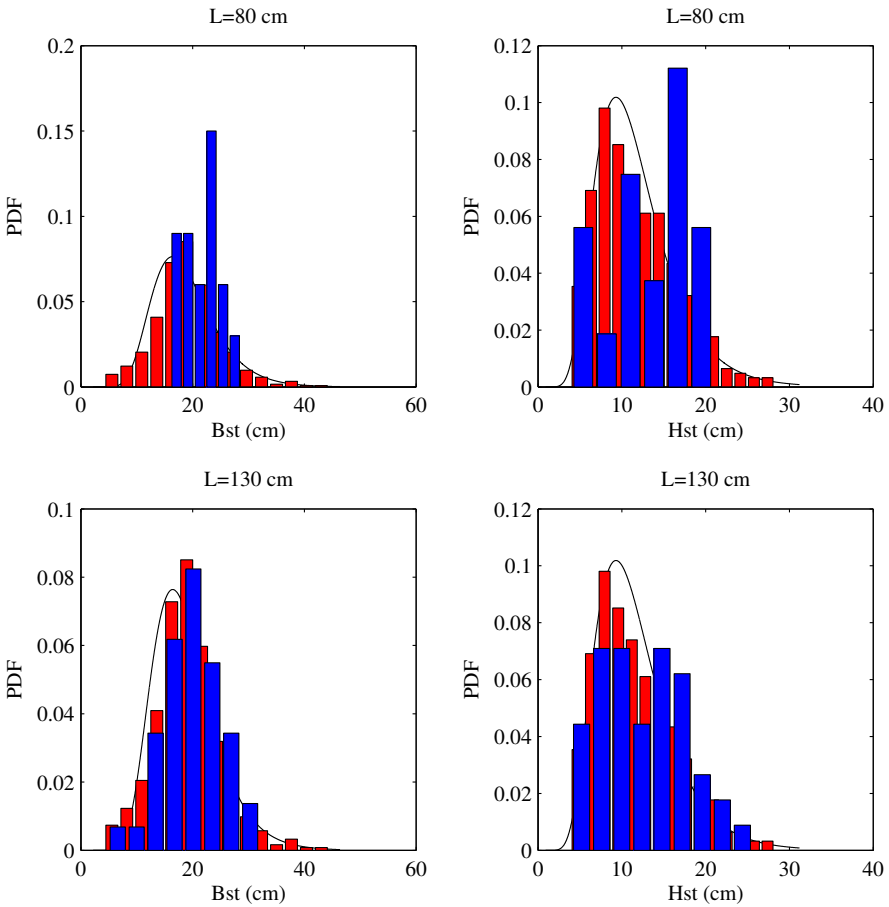


Figure 14. Comparison among probability density functions (PDF) of the width and the height of the stones relative to the windows (blue bars) with $L = 80$ cm and with $L = \hat{L} = 130$ cm, the entire masonry wall (red bars), and the log-normal curve (see Figure 3).

In particular, the difference in mean autocorrelation functions of the rows between the 130 cm window $\bar{A}C_{R,R}^{\hat{L}}(\xi)$ and the entire wall $\bar{A}C_{RR}(\xi)$ proved to be limited; see Figure 16 (A).

A similar result was obtained for the difference in mean autocorrelation functions of the columns: $\bar{A}C_{C,C}^{\hat{L}}(\eta)$ and $\bar{A}C_{C,C}(\eta)$, respectively; see Figure 16 (B).

Further studies would be necessary to gauge the importance of higher-order statistical properties. In any case, the elastic moduli of the equivalent homogeneous continuum are related to the average values of the strain and stress, and,

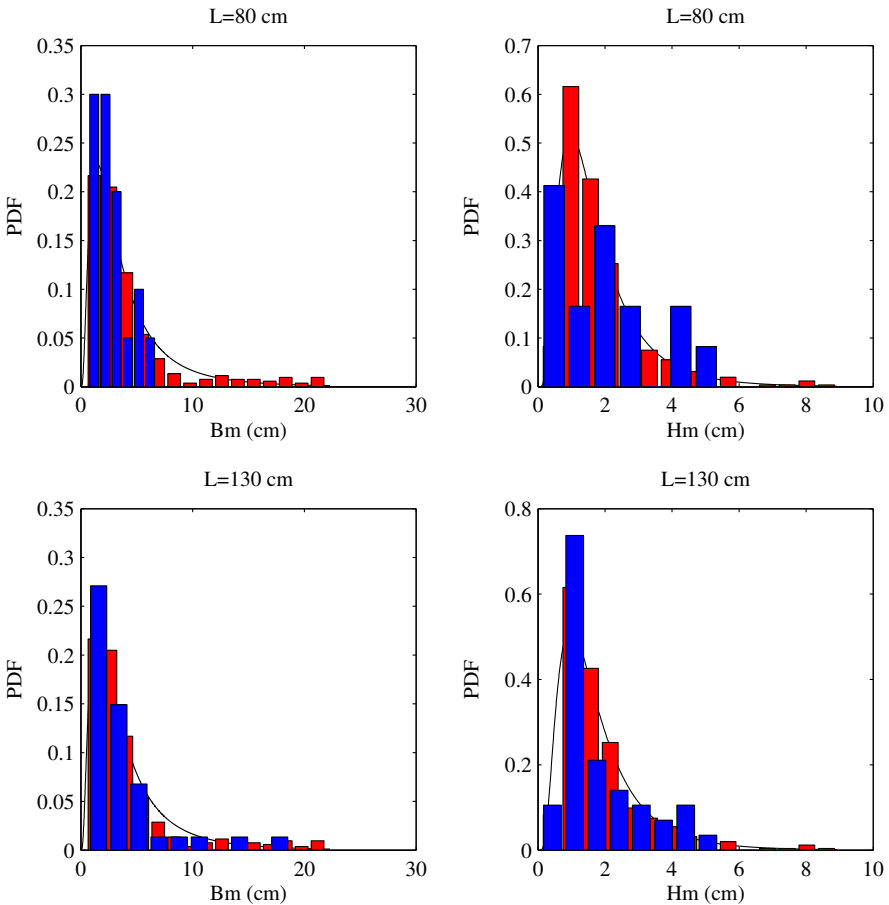


Figure 15. Comparison among probability density functions (PDF) of the characteristics of the mortar joints relative to the windows (blue bars) with $L = 80$ cm and with $L = \hat{L} = 130$ cm, the entire masonry wall (red bars), and the log-normal curve (see Figure 4).

consequently, the checks based on the proposed statistical descriptors would seem to be adequate.

Finally, by taking into account the mechanical and statistical results presented above, it becomes possible to consider the 130 cm window an adequate estimate of the statistically equivalent representative volume element, so that

$$T_{ij}^{\text{hom}} = T_{ij}^{\text{RVE}} = T_{ij, \hat{L}}^* = \frac{T_{ij, \hat{L}}^e + T_{ij, \hat{L}}^n}{2}, \quad \hat{L} = 130 \text{ cm.} \quad (42)$$

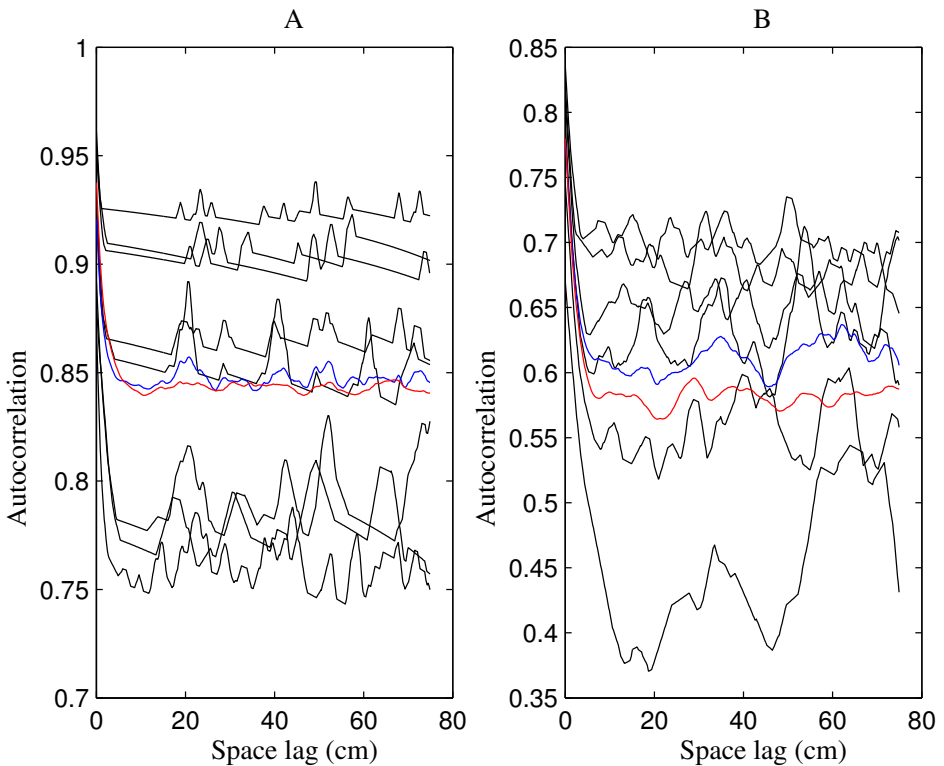


Figure 16. (A) Autocorrelation functions of the rows of the window with $\hat{L} = 130$ cm; mean autocorrelation functions: $\bar{A}C_{R,R}^{\hat{L}}(\xi)$ for the window (blue line), $\bar{A}C_{RR}(\xi)$ for the wall (red line); (B) Autocorrelation functions relative to the columns of the window with $\hat{L} = 130$ cm; mean autocorrelation functions: $\bar{A}C_{C,C}^{\hat{L}}(\eta)$ for the window (blue line), $\bar{A}C_{C,C}(\eta)$ for wall (red line).

6. Conclusions

This paper deals with the homogenization of masonry with nonperiodic microstructures. The masonry is treated as a random heterogeneous material and statistical descriptors are introduced. On the basis of observations concerning masonry construction, an orthogonal grid of rows and columns is used to determine the geometric characteristics of stones and of head- and bed-mortar joints. This allows one to estimate the statistical moments and the probability density function of these geometrical characteristics.

It is well known that the mechanical behavior of masonry is significantly influenced by its texture. In order to describe this feature, indicator (or characteristic)

functions are introduced to describe the random alternation of stone and mortar in the rows and columns of the orthogonal grid. Moreover, shifted-area functions and correlation functions are taken into account to highlight the random features of the masonry texture.

The modeling of the masonry as a random field was introduced to permit one to improve the finite-size test-window method in estimating the representative volume and the elastic moduli of the equivalent homogeneous medium. Since the classic mechanical criterion, which requires that differences between moduli evaluated under essential and natural conditions be limited, does not assure a uniform convergence of the test-window to the representative volume element, a probabilistic criterion is introduced.

This convergence criterion requires that the material window be statistically similar to the complete masonry wall, where this similarity is assured by the minimizing of differences among the statistical descriptors relative to the window and the entire masonry wall.

When both of these criteria are respected, the window can be considered an adequate estimate of the statistical equivalent representative volume, and the homogeneous continuum moduli can be obtained by averaging those relative to essential and natural boundary conditions.

A numerical application highlights the importance of applying the two criteria jointly and the effectiveness of the method proposed.

References

- [Alpa and Monetto 1994] G. Alpa and I. Monetto, “[Microstructural model for dry block masonry walls with in-plane loading](#)”, *J. Mech. Phys. Solids* **42**:7 (1994), 1159–1175.
- [Anthoine 1995] A. Anthoine, “[Derivation of the in-plane elastic characteristics of masonry through homogenization theory](#)”, *Int. J. Solids Struct.* **32**:2 (1995), 137–163.
- [Bensoussan et al. 1978] A. Bensoussan, J.-L. Lions, and G. Papanicolau, *Asymptotic analysis for periodic structures*, North-Holland, Amsterdam, 1978.
- [Bochenek and Pyrz 2004] B. Bochenek and R. Pyrz, “[Reconstruction of random microstructures – a stochastic optimization problem](#)”, *Comput. Mater. Sci.* **31**:1-2 (2004), 93–112.
- [Cecchi and Sab 2002] A. Cecchi and K. Sab, “[A multi-parameter homogenization study for modeling elastic masonry](#)”, *Eur. J. Mech. A: Solids* **21**:2 (2002), 249–268.
- [Christensen 1980] R. Christensen, *Mechanics of composite materials*, Wiley, New York, 1980.
- [Cluni and Gusella 2004] F. Cluni and V. Gusella, “[Homogenization of non-periodic masonry structures](#)”, *Int. J. Solids Struct.* **41**:7 (2004), 1911–1923.
- [De Buhan and De Felice 1997] P. De Buhan and G. De Felice, “[A homogenization approach to the ultimate strength of brick masonry](#)”, *J. Mech. Phys. Solids* **45**:7 (1997), 1085–1104.
- [Drugan and Willis 1996] W. Drugan and J. Willis, “[A micromechanics-based nonlocal constitutive equation and estimates of representative volume element size for elastic composites](#)”, *J. Mech. Phys. Solids* **44**:4 (1996), 497–524.

- [Hill 1963] R. Hill, “Elastic properties of reinforced solids: some theoretical principles”, *J. Mech. Phys. Solids* **11**:5 (1963), 357–372.
- [Huet 1990] C. Huet, “Application of variational concepts to size effects in elastic heterogeneous bodies”, *J. Mech. Phys. Solids* **38**:6 (1990), 813–841.
- [Luciano and Sacco 1997] R. Luciano and E. Sacco, “Homogenization technique and damage model for old masonry material”, *Int. J. Solids Struct.* **34**:24 (1997), 3191–3208.
- [Maier et al. 1991] G. Maier, A. Nappi, and E. Papa, “On damage and failure of brick masonry”, pp. 223–245 in *Experimental and numerical methods in earthquake engineering* (Ispra, 1991), edited by J. Donea and P. M. Jones, Kluwer, Dordrecht, 1991.
- [Ostoja-Starzewski 1998] M. Ostoja-Starzewski, “Random field models of heterogeneous materials”, *Int. J. Solids Struct.* **35**:19 (1998), 2429–2455.
- [Pande et al. 1989] G. Pande, J. X. Liang, and J. Middleton, “Equivalent elastic moduli for brick masonry”, *Comput. Geotech.* **8**:3 (1989), 243–265.
- [Pietruszczak and Niu 1992] S. Pietruszczak and X. Niu, “A mathematical description of macroscopic behaviour of brick masonry”, *Int. J. Solids Struct.* **29**:5 (1992), 531–546.
- [Povirk 1995] G. L. Povirk, “Incorporation of microstructural information into models of two-phase materials”, *Acta Metall. Mater.* **43**:8 (1995), 3199–3206.
- [Sab 1992] K. Sab, “On the homogenization and the simulation of random materials”, *Eur. J. Mech. A: Solids* **11**:5 (1992), 585–607.
- [Sab and B. 2005] K. Sab and N. B., “Periodization of random media and representative volume element size for linear composites”, *C. R. Mecanique* **333**:2 (2005), 187–195.
- [Sanchez-Palencia 1980] E. Sanchez-Palencia, *Non homogeneous media and vibration theory*, Lecture Notes in Physics **127**, Springer, Berlin, 1980.
- [Suquet 1987] P. M. Suquet, “Elements of homogenization for inelastic solid mechanics”, in *Homogenization techniques for composite media* (Udine, 1985), edited by E. Sanchez-Palencia and Z. A., Lecture Notes in Physics **272**, Springer, Berlin, 1987.
- [Terada et al. 2000] K. Terada, M. Hori, T. Kyoya, and N. Kikuchi, “Simulation of the multi-scale convergence in computational homogenization approaches”, *Int. J. Solids Struct.* **37**:16 (2000), 2285–2311.
- [Torquato 2001] S. Torquato, *Random heterogeneous materials*, Springer, New York, 2001.
- [Torquato and Stell 1982] S. Torquato and G. Stell, “Microstructure of two-phase random media, I: The n -point probability functions”, *J. Chem. Phys.* **77**:4 (1982), 2071–2077.
- [Šejnoha and Zeman 2002] M. Šejnoha and J. Zeman, “Overall viscoelastic response of random fibrous composites with statistically quasi uniform distribution of reinforcements”, *Comput. Methods Appl. Mech. Eng.* **191**:44 (2002), 5027–5044.
- [Šejnoha et al. 2004] M. Šejnoha, J. Zeman, and J. Novak, “Homogenization of random masonry structures, comparison of numerical methods”, pp. 13–16 in *17th ASCE Engineering Mechanics Division Conference* (Newark (DE), 2004), edited by J. T. Kirby et al., University of Delaware, Newark, 2004.
- [Zeman and Šejnoha 2001] J. Zeman and M. Šejnoha, “Numerical evaluation of effective elastic properties of graphite fiber tow impregnated by polymer matrix”, *J. Mech. Phys. Solids* **49**:1 (2001), 69–90.

Received 2 Nov 2005. Revised 17 Dec 2005.

VITTORIO GUSELLA: guse@unipg.it

*Department of Civil and Environmental Engineering, University of Perugia, Via G. Duranti,
Perugia 06125, Italy*

FEDERICO CLUNI: f.cluni@tiscali.it

Via Cima 36, fraz. Cerqueto, Marsciano (PG) 06052, Italy